Perturbation dynamics of a planktonic ecosystem

by Katherine Healey[1,2,3], Adam H. Monahan[1], and Debby Ianson[1,4]

ABSTRACT

Planktonic ecosystems provide a key mechanism for the transfer of carbon from the atmosphere to the deep ocean via the so-called "biological pump." Mathematical models of these ecosystems have been used to predict CO_2 uptake in surface waters at particular locations, and more recently have been embedded in global climate models. While the equilibrium properties of these models are well studied, less attention has been paid to their response to external perturbations, despite the fact that as a result of the variability of environmental forcing such ecosystems are rarely, if ever, in equilibrium. In this study, linear theory is used to determine the structure of perturbations to state variables of an ecosystem model describing summertime conditions at Ocean Station P (50°N 145°W) that maximize either instantaneous or integrated export flux. As a result of the presence of both direct and indirect pathways to export in this model, these perturbations involve the dynamics of the entire ecosystem. For all "optimal" perturbations considered, it is found that the flux to higher trophic levels is the primary contributor to export flux, followed by sinking detritus. In contrast, the contribution of aggregation is negligible. In addition, small phytoplankton contribute significantly (comparable to large phytoplankton) to the export flux through indirect pathways, primarily through the microzooplankton, even following a bloom in only large phytoplankton. While the details of these results may be specific to the particular model under consideration, the optimal perturbation framework is general and can be used to probe the dynamics of any mechanistic ecosystem model.

1. Introduction

Atmospheric carbon dioxide (CO_2) dissolves in the surface waters of the oceans and phytoplankton fix some of this carbon through photosynthesis, transforming it into particulate organic carbon (POC). A portion of this POC, denoted exported carbon, eventually reaches the deep ocean, where it remains essentially out of contact with the atmosphere on climatically significant time scales (i.e., 10^3 years). This process is known as the "biological pump," and enhances the ocean's ability to store carbon (e.g., Volk and Hoffert, 1985; Sarmiento and Gruber, 2006).

1. School of Earth and Ocean Sciences, University of Victoria, Victoria, British Columbia, V8W 3P6, Canada
2. Present address: Ecofish Research Ltd., 450 8th Street, Courtenay, British Columbia, V9N 1N5, Canada
3. Corresponding author. *email: khealey@ecofishresearch.com*
4. Fisheries and Oceans Canada, Institute of Ocean Sciences, Sidney, British Columbia, V8L 4B2, Canada

There are large areas of the ocean where major nutrients (e.g., nitrogen) are not normally drawn down to limiting concentrations by primary production. These are called high nutrient low chlorophyll (HNLC) regions, and include the subarctic North Pacific and Southern Ocean (de Baar *et al.*, 2005). Martin *et al.* (1989, 1991) hypothesized that phytoplankton growth in HNLC regions is limited by the micronutrient iron, and it has been suggested that atmospheric CO_2 may be reduced by fertilizing HNLC areas with iron to enhance the biological pump. An increase in phytoplankton biomass has been observed following both natural (e.g., Jo *et al.*, 2007) and synthetic (e.g., Saito *et al.*, 2006) iron fertilization events, however exported carbon in response to these events may only be measured indirectly (e.g., Wong *et al.*, 2006). In general, blooms such as these have not been occupied long enough to observe responses in export; thus the effect of iron fertilization on export dynamics remains uncertain.

Because of the importance of export dynamics and possible changes to these dynamics under climate change, it is necessary to develop mechanistic and predictive models of planktonic ecosystems. Such models typically consist of a system of differential equations describing the temporal evolution of ecosystem variables (e.g., nutrients, phytoplankton, zooplankton; Fasham, 1993). Real planktonic systems involve a large number of species displaying a bewildering complexity of physiological states, nutrient requirements, and trophic interactions. Rather than attempt to represent explicitly all of these complex interactions, planktonic ecosystem models make use of a number of simplifying approximations. In particular, phytoplankton and zooplankton are divided into what are termed 'functional groups,' defined by common ecosystem-scale characteristics.

Many formulations for modeling ecosystem dynamics have been proposed, ranging in complexity from three state variables (nutrient, phytoplankton (P), zooplankton (Z)) in a homogeneous medium without explicit spatial structure (e.g., Steele, 1974) to spatially three-dimensional models containing multiple functional groups of plankton and nutrients (e.g., Moore *et al.*, 2004). In addition, many comprehensive global climate models that are used to study climate change have an ocean biology component that includes a simple planktonic ecosystem model (e.g., Schmittner *et al.*, 2005; Zahariev *et al.*, 2008). However, the dynamics of these ecosystem models - particularly their response to a variable physical environment - are often poorly understood. Coupled physical-biological ecosystem models have suggested that physical variability can induce significant changes in primary and secondary production, the distribution between small and large phytoplankton, and carbon export (e.g., McGillicuddy *et al.*, 1995; Friedrich and Hofmann, 2001; Leising *et al.*, 2003; Monahan and Denman, 2004).

While the nonlinearity of these model equations generally limits the full analytical study of model dynamics, useful insight can often be obtained through the study of dynamics linearized locally around model equilibria (e.g., Perko, 2001). Continual physical forcing from the atmosphere and ocean mean that these ecosystems are never in steady state (Monahan and Denman, 2004, hereafter referred to as MD04). If variability is not too large, the state of the ecosystem may be considered as a steady background state that is modified

by some perturbation evolving according to locally linear dynamics. Such a linearization allows for a systematic analysis of the model dynamics for a small perturbation from steady state, and may provide qualitative information about the behaviour of perturbations that may not be considered "small." Locally linearized dynamics have been used to study the stability properties of model equilibria (e.g., Edwards and Brindley, 1999), but although it has been demonstrated that modeled phytoplankton populations can display rapid transient growth (e.g., Pitchford and Brindley, 1999; Truscott and Brindley, 1994), little attention has been paid to the dynamics of perturbations around steady states. The relationship between the evolution of ecosystems and export flux is complicated, and possibly counter-intuitive. Well established mathematical theory (e.g., Tziperman and Ioannou, 2002) may be used to determine perturbations to a steady state that lead to responses from the ecosystem that are "optimal" in some specified way, such as maximizing the export flux (rate of POC leaving the model domain). These perturbations represent small changes to an ecosystem state that may occur in response to external forcing by natural occurrences such as addition of iron by dust deposition, advection and mixing with an eddy that has a different concentration of state variables, or mixed layer depth variability in response to fluctuating atmospheric forcing.

This study considers the dynamics of a medium complexity (five variable) model, designed to simulate ecosystem processes at Ocean Station P (50°N 145°W). Ocean Station P is an HNLC region located in the subarctic northeast Pacific, where spring and summer-time photosynthetic growth is thought to be limited by micronutrients such as iron. In this region, small phytoplankton are dominant and tightly coupled with microzooplankton, and diatom blooms are observed only occasionally (Boyd and Harrison, 1999). A wealth of historical data exist (Whitney and Tortell, 2006), and Station P was the site of the Subarctic Ecosystem Response to Iron Enrichment Study (SERIES), a synthetic iron fertilization experiment (Boyd *et al.*, 2004). The historical data show that chlorophyll remains approximately constant throughout the year despite considerable variability within the ecosystem (Wong *et al.*, 1999). Most of the time, the ecosystem at Station P appears to be near, or fluctuating about, steady state, and thus this setting is ideal for the analysis of small perturbations around equilibrium.

While this model is a highly idealized representation of the natural ecosystem, it is representative of the type of model currently being embedded in global climate models, so its dynamics are of interest for their implications regarding the ecosystem and these complex global models. The model is presented in Section 2, ecosystem and export responses to perturbations are presented in Section 3, and results are discussed in Section 4. Model details, export, and linear optimization theory are discussed in Appendixes A, B, and C, respectively.

2. Model

The planktonic ecosystem model used in this study is based on MD04 (Fig. 1), but without explicit spatial structure, i.e., in a uniform mixed layer of fixed depth. The ecosystem
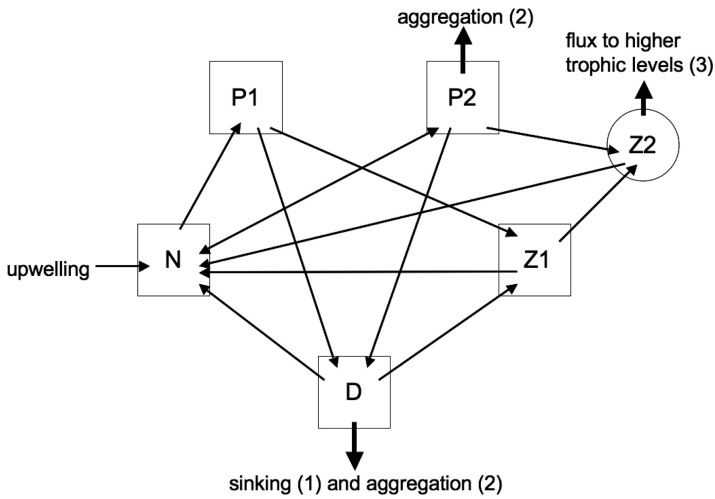
Figure 1. Model dynamics. State variables include nitrogen (N), small phytoplankton (P1), large phytoplankton (P2), small zooplankton (Z1), large zooplankton (Z2, prescribed), and detritus (D). Bold arrows denote export: detritus sinks (1), detritus and large phytoplankton form aggregates (2), and large phytoplankton and small zooplankton are consumed by large zooplankton (3). In steady state these losses are balanced by the input of *N* via upwelling.

model is similar to those used in global models of the carbon cycle (e.g., Zahariev *et al.*, 2008). There are two functional groups of phytoplankton; small ($\leq 20\,\mu m$) phytoplankton, including flagellates (P_1), and large ($> 20\,\mu m$) phytoplankton, mainly diatoms (P_2). The phytoplankton are divided into two functional groups because small and large phytoplankton are grazed upon by different trophic levels, and P_2 are normally thought to be the most important contributor to export flux (Michaels and Silver, 1988). Microzooplankton (Z_1) are modeled explicitly, and are tightly coupled with their prey: small phytoplankton and dead organic matter, termed detritus (*D*). Mesozooplankton (Z_2) graze on larger prey (in this model P_2 and Z_1); time scales for changes in Z_2 biomass are much longer than for phytoplankton and microzooplankton, and thus Z_2 is specified at a constant value (the maximum value of the observed annual cycle (Goldblatt *et al.*, 1999) in order to simulate summer conditions). The model is set in an HNLC region so nitrogen is not limiting; instead, a constant iron limitation factor, L_{Fe}, is applied to limit photosynthetic growth rates. Although it is not limiting and therefore does not influence the other components of the model, nitrogen (*N*) is influenced by perturbations to the planktonic components and therefore is explicitly modeled. A full mathematical description of the ecosystem model is given in Appendix A. Table 1 contains definitions of symbols that are frequently used in this study, including state variables. As a convenient shorthand, we will use the state variables P_1, P_2, Z_1, *D* to refer to both the planktonic/detrital functional types and the corresponding biomasses; the appropriate meaning will be clear from the context.

Table 1. Definition of frequently used symbols. Each Φ represents a perturbation experiment.

t	Time
P_1	Small phytoplankton ($\leq 20\,\mu$m)
P_2	Large phytoplankton ($> 20\,\mu$m)
Z_1	Microzooplankton
D	Detritus
N	Nitrogen
Z_2	Mesozooplankton
Φ_{FLUX}	Maximizes instantaneous export flux, amplification
Φ_{FLUX-P}	Maximizes instantaneous export flux, amp.; restricted to P_1 and P_2
Φ_{INT}	Maximizes integrated export
Φ_{P_2}	Increase in only P_2
$\Phi_{P_1 P_2}$	Proportional increase in P_1 and P_2
Φ_{P_1}	Increase in only P_1

Previous experiments have found a steady state configuration for this model (Table 2) that is stable and able to recover from reasonably small perturbations (Healey, 2008). This steady state also corresponds to a reasonable representation of conditions at Station P. While this steady state is asymptotically stable, some perturbations may display growth over finite times. That is: although perturbations must eventually decay, they may initially grow. The perturbation dynamics around this equilibrium will be the focus of this study. Perturbations (of initial magnitude $1\,\mathrm{mmol\,N\,m^{-3}}$) that maximize export flux from the ecosystem are determined (see Appendix C for methods), and responses to perturbations that display the highest export flux, relative to the initial export flux, are presented and discussed in Section 3. Note that because we consider the linearized model dynamics, the evolution of the perturbations is insensitive to the initial perturbation magnitude.

There are three pathways for the export of particulate matter from the ecosystem: sinking D (with no aggregation), flux to higher trophic levels as P_2 and Z_1 are grazed upon by Z_2, and aggregation of P_2 and D (Fig. 1 bold arrows, Eq. (1)). The third export pathway simulates the formation of marine snow in which larger phytoplankton and detritus form aggregates, which then sink (Alldredge and Silver, 1988). Also note the implicit assumption that the matter going to higher trophic levels does not re-enter the surface layer of the ocean.

Note that the analyses in this study consider only export of particulate organic carbon and neglect contributions of dissolved organic carbon to export flux. This assumption is

Table 2. Ecosystem state variable values for the only stable steady state of the 4 steady state solutions possible.

		steady state values ($\mathrm{mmol\,N\,m^{-3}}$)		
P_1	P_2	Z_1	D	N
0.5265	0.1105	0.4073	0.0919	8.3153

Table 3. Unit perturbations (mmol N m^{-3}) to steady state. The perturbation Φ_{FLUX} is in all state variables, maximizes instantaneous export flux, and gives high transient amplification. The perturbation Φ_{FLUX-P} is only in phytoplankton state variables, maximizes instantaneous export flux, and results in significant amplification. The perturbation Φ_{INT} maximizes integrated export flux. The perturbations Φ_{P_2}, $\Phi_{P_1 P_2}$, and Φ_{P_1} are considered for comparison to the optimal perturbations. These perturbations have been scaled to magnitude 0.5 mmol N m^{-3} in the present analysis.

	P_1	P_2	Z_1	D	N
Φ_{FLUX}	0.0785	0.8160	−0.5641	−0.0989	−0.0005
Φ_{FLUX-P}	0.6423	0.7665	0	0	0
Φ_{INT}	−0.0009	0.9977	−0.0296	0.0616	−0.0040
Φ_{P_2}	0	1.0000	0	0	0
$\Phi_{P_1 P_2}$	0.9807	0.1955	0	0	0
Φ_{P_1}	1.0000	0	0	0	0

reasonable as a first approximation; sediment trap data suggest that POC is the greatest contributor to export flux at 20 m at Station P (Wong *et al.*, 1999).

Export from the ecosystem is given by the equation

$$Export = w_D D + (1 - m_{ca})\gamma_2 Z_2 + w_A (P_2 + D)^2 \tag{1}$$

where w_D is the rate of sinking D, m_{ca} the Z_2 excretion rate, γ_2 the Z_2 grazing rate, and w_A the aggregation coefficient. In order to perform the optimizations (Appendix C), this equation must be linearized about the steady state. The linearized export in this case is given by

$$Export = Export(\mathbf{x}_0) + 0.22\Delta P_2 + 0.21\Delta Z_1 + 0.38\Delta D \tag{2}$$

where $\mathbf{x}_0$ is the steady state vector and ΔP_2, ΔZ_1, and ΔD are the perturbations in large phytoplankton, small zooplankton, and detritus, respectively. Further detail on export is presented in Appendix B.

3. Results: Ecosystem and export flux responses to perturbations

For the linearized dynamics considered in this analysis, the character of the response to an initial perturbation is independent of the size of this perturbation (apart from an overall scale factor). For illustrative purposes, we have scaled initial perturbations in Table 3 to be of magnitude 0.5 mmol N m^{-3}. This perturbation magnitude is at the upper end of the range of values over which the linearized dynamics are a reasonable approximation to the fully nonlinear dynamics (Healey, 2008).

a. Export flux

As discussed in Appendix C, we determine perturbations of specified initial magnitude to the model steady state that maximize the instantaneous export fluxes for the linearized
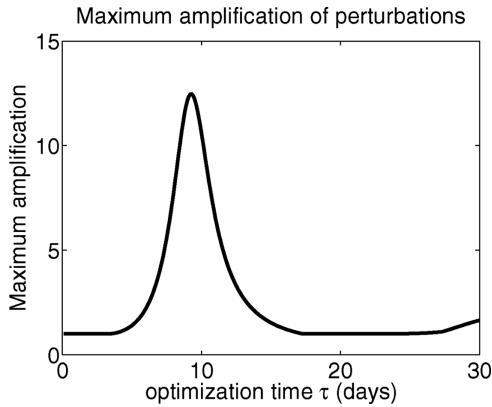
Figure 2. Maximum amplification of export flux following perturbations in all state variables that maximize export flux at time τ. The perturbation that gives the maximum amplification is Φ_{FLUX} and corresponds to the perturbation that maximizes export flux at $\tau = 9.3$ days.

model at specified times τ. These "optimal perturbations" are calculated ten times per day for fixed times between 0 and 30 days, so that there is sufficient resolution to observe the dependence of optimal perturbations on optimization time. Of the perturbations that maximize instantaneous export flux, the perturbation that results in the largest amplification (maximum instantaneous export flux relative to the initial export flux; given by Eq. (20)) is the perturbation that maximizes the export flux for $\tau = 9.3$ days, with a maximum amplification factor of 12.5 (Fig. 2). The set of changes to the state variables in this case is referred to as Φ_{FLUX}, and its components are given in Table 3.

i. Ecosystem response. The linearized response to Φ_{FLUX} is shown in Figure 3a. This initial perturbation consists primarily of an increase in P_2 (Table 3), that monotonically decreases, taking 75 days to drop to 10% of its initial value, and a decrease in Z_1 that allows a rapid bloom of P_1 which peaks at day 6.

The Z_1 recover due to the abundance of available food, reaching maximum biomass at day 11. The P_1 are then grazed below steady state value to a minimum at day 17, which leads to a local minimum of Z_1 occurring at day 22. Damped predator-prey oscillations (Volterra, 1928) continue to occur with a period of 22-23 days, with the P_1 leading the Z_1 by five to six days. Because the model has more than two dimensions, predator-prey oscillations are not required to be about steady state; for most of the evolution of the perturbation, the P_1 remain above steady state value as the ecosystem approaches equilibrium, while Z_1 biomass oscillates about the steady state. The initial perturbation in P_1 is negligible, so that P_1 and Z_1 are synchronized relative to their predator-prey oscillation cycle with a lag of five days, allowing the maximum response in P_1.

Detritus biomass, and thus export flux of sinking D, reaches a maximum at nine days, after the initial P_1 bloom peaks but before the Z_1 attain their maximum. This maximum of
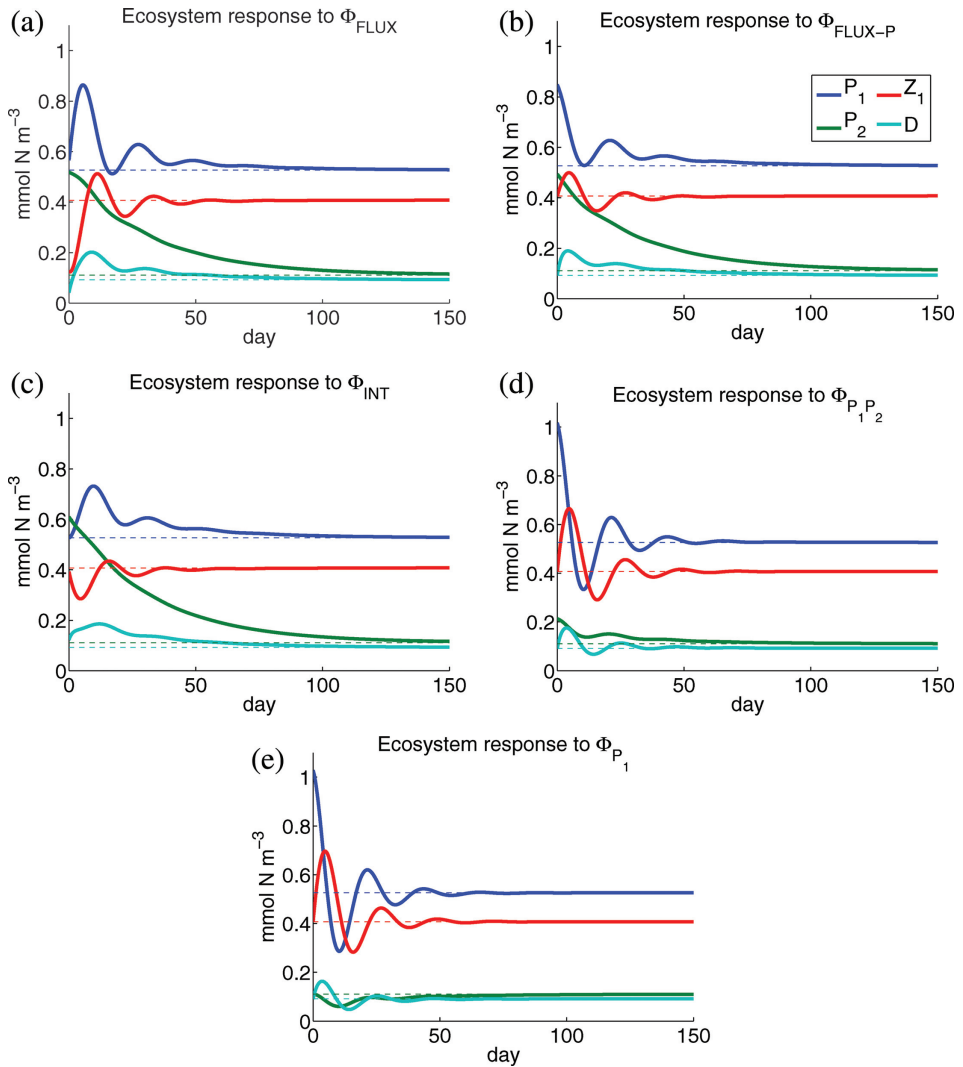
Figure 3. Linearized ecosystem response to perturbations Φ_{FLUX} (a), Φ_{FLUX-P} (b), Φ_{INT} (c), $\Phi_{P_1 P_2}$ (d), and Φ_{P_1} (e) for the first 150 days following the perturbation at $t = 0$. The dashed lines show the steady state values for each state variable. In each panel, dark blue is P_1, green is P_2, red is Z_1, and teal is D.

D occurs before the peak Z_1 for two reasons: a portion of the increased P_1 being grazed down by Z_1 enters the D pool via 'sloppy feeding', and there is less grazing of Z_1 on D at this time (Eq. (5)).

There is considerable drawdown in N (2-3 μM) with the concentration decreasing to a minimum of less than 6 μM at 68.5 days (Fig. 4). This decay in N results from the balance

between P_2 uptake, with a long decay time, and the slow, steady supply of N from below. After this time, N concentrations begin to increase, albeit slowly, taking over a year to approach the former steady state value. In fact, the model dynamics governing incoming N are unrealistic: all N recovery is through upwelling and diffusion, as the model does not include horizontal mixing of nutrients. Furthermore, the model is set in a perpetual summer, with no winter deepening of the mixed layer. However, because the ecosystem is not N limited at any time, the N dynamics have no effect on the other state variables or export dynamics, which is the primary focus of this analysis.

ii. Export response. All components of export flux increase initially in response to Φ_{FLUX} (Fig. 5a). Export flux due to aggregation reaches a maximum at day 6, after the maximum in P_2 and before the maximum in D, and then decreases toward steady state. Export to higher trophic levels reaches a maximum at day 10, and net export increases to a maximum shortly before day 10, reflecting a compromise between export due to sinking D and flux to higher trophic levels. These maxima follow the maximum in P_1; increased grazing on P_1 produces D, which sinks and contributes to aggregation, and the increased Z_1 biomass increases the flux to higher trophic levels. The maximum aggregation occurs earliest, before P_2 mortality increases due to increased grazing of Z_2 on Z_1. There is a second peak in export flux around day 30, and export fluxes display damped oscillations on the time scale of predator-prey interactions, in response to these oscillations in P_1 and Z_1.

Both major export events follow blooms in P_1. The maximum instantaneous export flux is 4.4 mmol N m^{-2} d^{-1} (Table 4), the highest instantaneous export flux in response to any of the perturbations. Note that by construction, Φ_{FLUX} is the perturbation that gives the highest export flux relative to the initial export flux of the perturbation, with an amplification factor of 12.5 (Fig. 6). The additional integrated export above steady state in response to this perturbation is 76 mmol N m^{-2} (6.1 g C m^{-2} assuming a C:N ratio of 106:16, see Appendix B) over 150 days. Aside from the initial decreased flux of sinking detritus, all export rates remain above steady state export rates, primarily because P_1 and P_2 remain above their mean values.

b. Export flux, perturbation in P_1 and P_2

In the previous section, the optimal perturbations were permitted to involve all components of the ecosystem, and all model state variables were involved in mediating the responses to this perturbation. In particular, interactions between P_1 and Z_1 were seen to be an important aspect of the response. It is natural to ask how large a response can be generated from a perturbation in only the phytoplankton, such as a bloom. Thus, for this optimization (Appendix C), only perturbations in P_1 and P_2 were allowed, while Z_1, D, and N were held constant. The set of changes to the state variables in this case is referred to as Φ_{FLUX-P}

The initial perturbation is an increase in both P_1 and P_2 (Table 3), and thus immediately increases instantaneous export flux. This initial increase in export flux is considerably more
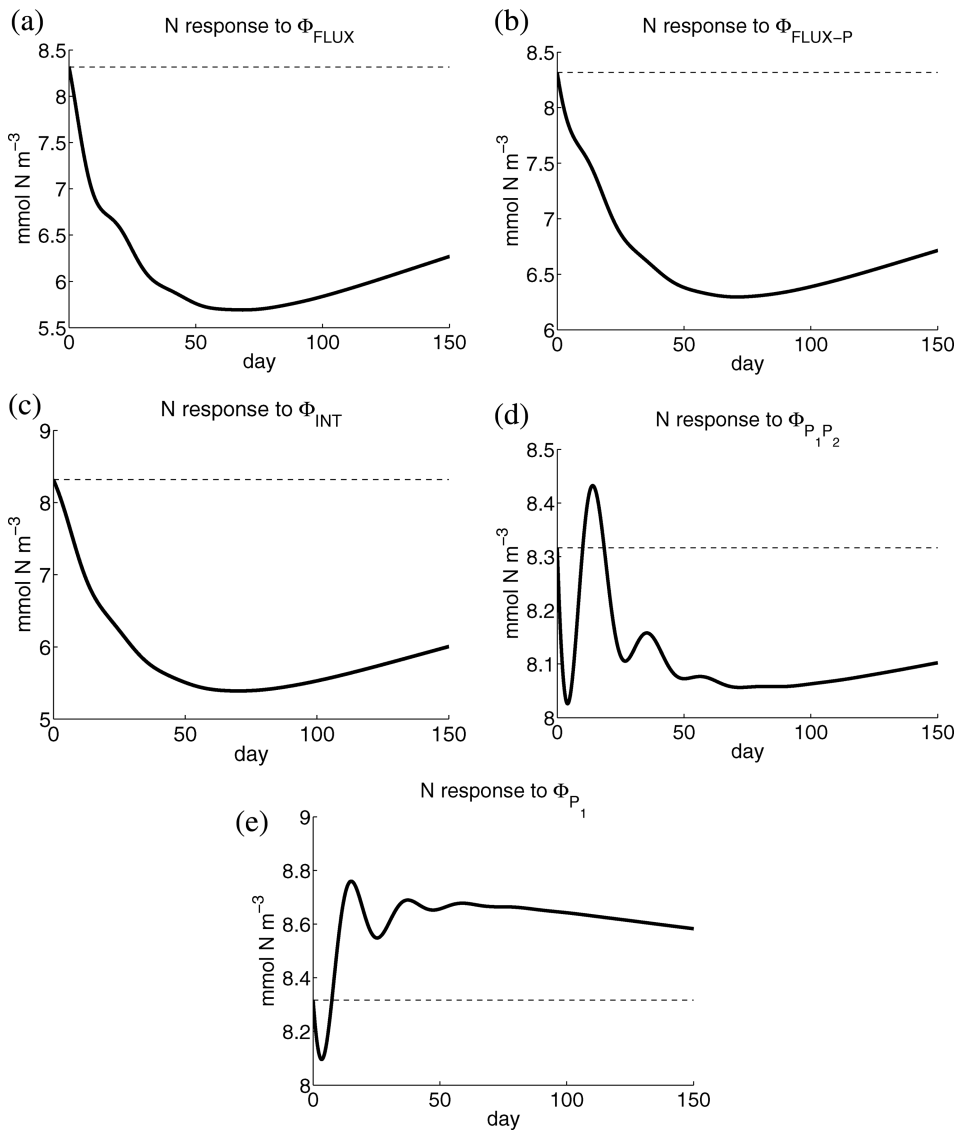
Figure 4. Linearized nitrogen response to perturbations Φ_{FLUX} (a), Φ_{FLUX-P} (b), Φ_{INT} (c), $\Phi_{P_1 P_2}$ (d), and Φ_{P_1} (e) for the first 150 days following the perturbation at $t = 0$. Dashed lines show value at steady state.

than in the case of Φ_{FLUX}, for which the increase in P_2 was partially offset by a decrease in Z_1. As a result, although the magnitudes of the transient export flux are comparable between these two cases (Table 4), the maximum amplification of the instantaneous export (at $\tau = 4.3$ days) for Φ_{FLUX-P} was much smaller (only 1.5) than for Φ_{FLUX}.
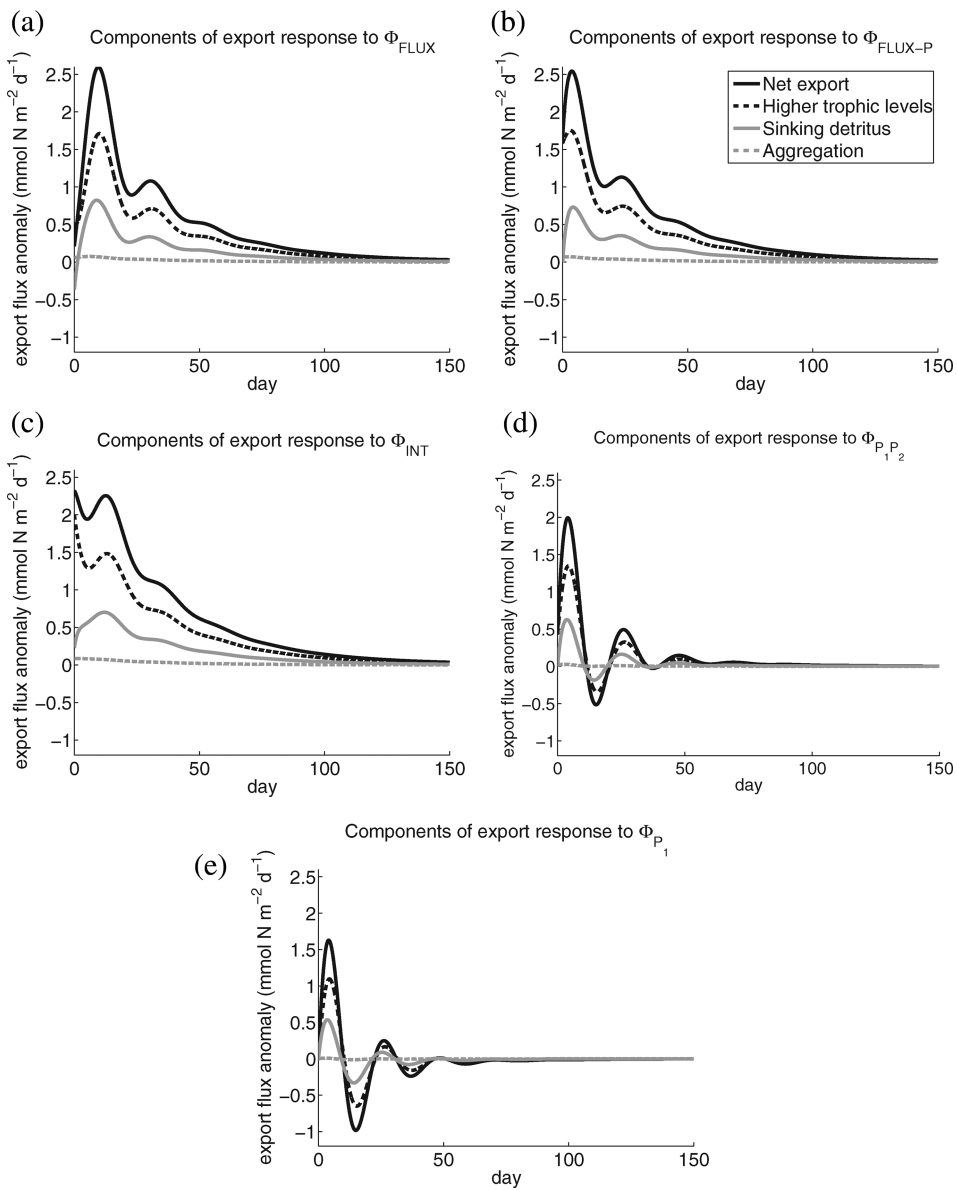
Figure 5. Linearized components of export flux anomaly (i.e., export flux anomaly at steady state is 0) in response to perturbations Φ_{FLUX} (a), Φ_{FLUX-P} (b), Φ_{INT} (c), $\Phi_{P_1 P_2}$ (d), and Φ_{P_1} (e) for 150 days following the perturbation at $t = 0$. The solid black line is net export, the solid grey line is sinking detritus, the dashed grey line is aggregation, and the dashed black line is flux to higher trophic levels.

Table 4. Properties of export responses to perturbations: minimum and maximum export flux, and integrated export over 150 days (1 hr timestep) in response to perturbations, for perturbation of magnitude 0.5 mmol N m^{-3}. The values in Column 4 are calculated using a Redfield ratio of 106:16 C:N. Export fluxes are obtained by multiplying export per unit volume by mixed layer depth (20 m). Column 5 represents the P_2 decay time.

	export flux (mmol N m^{-2} d^{-1})		int. export (mmol N m^{-2})	int. export relative to steady state (g C m^{-2})	day such that $\Delta P_2(t) =$ $.1\Delta P_2(0)$
	min	max			
Φ_{FLUX}	2.0	4.4	350	+6.1	75
Φ_{FLUX-P}	1.9	4.4	350	+5.7	73
Φ_{INT}	1.9	4.2	370	+7.4	75
Φ_{P_2}	1.9	4.1	370	+7.4	75
$\Phi_{P_1 P_2}$	1.3	3.8	300	+1.5	56
Φ_{P_1}	0.86	3.5	280	+0.02	NA
Steady State	1.8	1.8	280	0	NA

i. Ecosystem response. The ecosystem response to Φ_{FLUX-P} is shown in Figure 3b. This perturbation is an increase in both P_1 and P_2. The P_2 decay time scale is slightly shorter than in response to Φ_{FLUX}; perturbed P_2 take 73 days to decay to 10% of the initial perturbation. The response to this perturbation is very similar to the response to Φ_{FLUX} but shifted by about six days; like Φ_{FLUX}, damped predator-prey oscillations follow the perturbation, with P_1 remaining above steady state and Z_1 fluctuating about steady state.

ii. Export response. All components of export flux increase immediately following Φ_{FLUX-P} (Fig. 5b). The net export flux reaches a maximum at four days. While the export
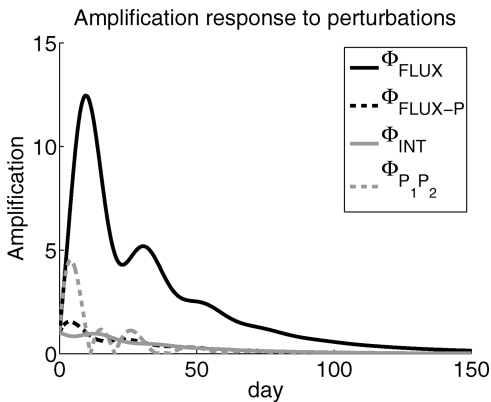

Figure 6. Amplification (dimensionless, Eq. (20)) in response Φ_{FLUX} (solid black), Φ_{FLUX-P} (dashed black), Φ_{INT} (solid grey), and $\Phi_{P_1 P_2}$ (dashed grey). The time of the perturbations is $t = 0$. Note that Φ_{P_1} is not included as amplification is infinite in response.

flux is dominated by flux to higher trophic levels, the magnitude of this flux decreases following the perturbation; sinking detritus increases significantly following the initial perturbation, and is the main contributor to the amplification of export. The initial perturbation does not change the amount of D present in the ecosystem, but increased D due to Z_1 grazing on P_1, and P_2 mortality, result in additional export of sinking D, to a maximum at four days. The additional integrated export in response to Φ_{FLUX-P} of 75 mmol N m^{-2} (5.7 g C m^{-2}) is slightly less than Φ_{FLUX} (Table 4).

c. Integrated flux

In the previous sections, instantaneous export flux was maximized at fixed times. These optimal perturbations may have little influence on the total amount of POC exported, as there is no guarantee that the transient export fluxes remain high as the ecosystem returns to equilibrium. The unit perturbation that maximizes the integrated export, i.e., the total amount of POC exported from the ecosystem as it returns to equilibrium, Φ_{INT}, is determined as presented in Appendix C.

i. Ecosystem response. The linearized ecosystem response to the perturbation Φ_{INT} is shown in Figure 3c. This perturbation is primarily an increase in P_2 (Table 3). The other components of the initial perturbation conditions have a negligible effect on the ecosystem and export response; the responses to Φ_{INT} are nearly indistinguishable from the responses to a perturbation that only increases P_2, Φ_{P_2} (Table 4). This initial increase in P_2 decays slowly, taking more than 75 days to drop below 10% of its initial value.

As the perturbation evolves, the initial slight decrease in Z_1 is amplified and the Z_1 biomass reduced significantly below equilibrium value to a minimum at 4.5 days. The increase in P_2 increases the overall grazing rate of Z_2, causing this decrease in Z_1. This response differs from the Z_1 increase observed following Φ_{FLUX} because Φ_{INT} has almost no P_1 component, so there is no initial increase in flux to Z_1 biomass to offset the increased Z_2 grazing. The decrease in Z_1 results in less predation on P_1, D, and P_2 (indirectly), and allows an increase in P_1 that peaks at 9.6 days. This bloom increases the food availability of the Z_1, which respond by recovering to above- steady state values, peaking at 15.8 days. Like the response to Φ_{FLUX}, damped predator-prey oscillations continue in P_1 and Z_1. At no time does the P_1 biomass drop below steady state, while the Z_1 biomass oscillates about its equilibrium value. Detritus values reach a maximum at 12.0 days.

ii. Export response. The perturbation Φ_{INT} is primarily an increase in P_2, which results in an immediate increased flux to higher trophic levels, and thus net export (Fig. 5c). The increased flux to higher trophic levels (Z_2 grazing) results in a decrease of Z_1, and a local minimum of both flux to higher trophic levels and net export. Damped oscillations driven by the predator-prey cycle between Z_1 and P_1 follow. Following the maxima caused by the initial P_1 bloom (which is a consequence of the initial decrease in Z_1), all export components decrease. At no time do any of the export rates drop below steady state values.

The perturbation Φ_{INT}, results in additional integrated export of $93\,\text{mmol N m}^{-3}$ ($7.4\,\text{g C m}^{-2}$, Table 4) about 20% greater than that of Φ_{FLUX}. The maximum export flux occurs at the time of perturbation, i.e., the maximum instantaneous amplification factor is less than 1. As in the response to Φ_{FLUX}, the slow decay of P_2, which is exported to higher trophic levels, is the primary reason for the large integrated export.

d. Non-optimal perturbation: Proportional increase in P_1 and P_2

The optimal perturbation in only P_1 and P_2, Φ_{FLUX-P}, resulted in increased integrated export from the ecosystem relative to steady state (Table 4), and was primarily an increase in P_2. To investigate the dependence of perturbation evolution on initial conditions of our choosing, we consider an instantaneous bloom in both functional groups, $\Phi_{P_1 P_2}$, represented by an increase in both P_1 and P_2 proportional to the phytoplankton steady state values (Table 3). Many conditions that improve conditions for photosynthesis for one phytoplankton functional group will similarly benefit other groups and also increase their growth rates, potentially resulting in an initial increase in both size classes proportional to steady state values. This perturbation was not determined by consideration of the optimality of export response, but rather is considered for comparison to the optimal perturbations.

i. Ecosystem response. The linearized ecosystem response to $\Phi_{P_1 P_2}$, shown in Figure 3d, is dominated by the predator-prey oscillations between Z_1 and P_1. Unlike the responses to Φ_{INT} and Φ_{FLUX}, the P_1 and Z_1 both drop below steady state levels. The P_2 anomaly decays by 71% to a relative minimum at 11.7 days. Weak oscillations follow, driven by the predator-prey cycle in P_1 and Z_1 (which influences Z_2 grazing rates). P_2 values do not drop below their steady state value at any time, and it takes about 56 days for the perturbed P_2 to decrease to 10% of the initial perturbation.

The N response to $\Phi_{P_1 P_2}$ is much different than the responses to Φ_{FLUX}, Φ_{FLUX-P}, and Φ_{INT}, which by construction, maximized exports. Initially N concentrations decrease as biological uptake exceeds incoming N from upwelling, reaching a minimum at 4.1 days. This change in N is much smaller than the response to previous perturbations. Afterward, N begins to increase rapidly while overall primary production decreases, reaching a maximum in excess of its steady state concentration at 14.0 days. Following this maximum, N decreases to below equilibrium, as primary production again increases above steady state.

ii. Export response. All of the export components initially increase following $\Phi_{P_1 P_2}$ (Fig. 5d), with a maximum overall amplification factor of 4.5, although this perturbation reduces export flux for short time intervals. The integrated export in response to $\Phi_{P_1 P_2}$ is $19\,\text{mmol N m}^{-2}$ ($1.5\,\text{g C m}^{-2}$), considerably less than the other perturbations discussed so far (Table 4). The maximum export flux in response to $\Phi_{P_1 P_2}$ is $3.8\,\text{mmol N m}^{-2}\,\text{d}^{-1}$, similar to the other perturbations, but unlike those previously discussed, the export flux oscillates around the steady state value of $1.8\,\text{mmol N m}^{-2}\,\text{d}^{-1}$, with a minimum export

flux of 1.3 mmol N m^{-2} d^{-1}. This different behavior occurs because the P_2 contribution to increased export flux relative to steady state is not large enough to offset the decrease in D and Z_1 contributions following the declines in P_1 blooms. These minima are responsible for the relatively low integrated export, which is 20% of the integrated export due to Φ_{INT}.

e. Non-optimal perturbation: Increase in P_1 alone

The perturbation $\Phi_{P_1 P_2}$ is primarily an increase in P_1 (Table 3). Integrated export resulting from this perturbation is low compared to that from the optimal perturbations, which are primarily in P_2, and is not much higher than the integrated export from the ecosystem at steady state. This difference led us to investigate if increasing only P_1 results in feedbacks that actually reduce the integrated export below that which occurs when the ecosystem remains at steady state over an equal time period. Like $\Phi_{P_1 P_2}$, this perturbation is not the result of an optimization, and will be referred to as Φ_{P_1}.

The ecosystem response to this perturbation, shown in Figure 3e, initially resembles that of $\Phi_{P_1 P_2}$, but at 7.4 days the N anomaly becomes positive and remains slightly above zero as it decays. The concentration of N decreases when primary production is above steady state, and increases during periods when primary production is below steady state. Because, in general, export flux is highest during and following periods of high primary production, N concentration tends to decrease before periods of enhanced export flux and increase during periods of reduced export flux.

The maximum instantaneous export flux in response to Φ_{P_1} is 3.5 mmol N m^{-2} d^{-1} (Table 4), similar to the other perturbations, although the minimum export flux is the lowest at 0.9 mmol N m^{-2} d^{-1}. There is one major export event in response to Φ_{P_1} (Fig. 5e), which is followed by a rapid decline in export flux. The integrated export in response to Φ_{P_1} is nearly the same as integrated export from an ecosystem in steady state over an equivalent time period (Table 4). A perturbation that increases only P_1 has effectively no impact on the net export.

4. Discussion

While there are significant differences in detail between the ecosystem responses to the different optimal and non-optimal perturbations considered in the previous section, these responses share a number of common features. In particular, the small phytoplankton and zooplankton (P_1 and Z_1) are tightly coupled because of their similar specific growth rates. This tight coupling results in predator-prey cycles (in five dimensions, so these oscillations do not always orbit around the steady state as would be the case in a two-dimensional system), and to indirect couplings between P_1 and P_2 mediated by the grazers. An increase in P_2 results in an increased mesozooplankton specific grazing rate such that the increased grazing pressure on Z_1 can lead to a decline in microzooplankton biomass and a consequent increase in P_1. In contrast, an increase in P_1 can lead to an increase in Z_1 and therefore to a *decrease* in P_2 due to increased grazing pressure by Z_2.

For the optimal perturbations, the P_1 biomass remains near or above steady state, resulting in enhanced fluxes to higher trophic levels. For the perturbation maximizing integrated export flux, Φ_{INT}, Z_1 biomass remains below or near steady state: the resulting reduction in grazing pressure on P_2 allows for a more persistent bloom and enhanced net export flux. Note that those perturbations optimizing instantaneous export flux (Φ_{FLUX}, Φ_{FLUX-P}) are associated with strong oscillatory variability in the $P_1 - Z_1$ sector; the resulting substantial "blooms" are responsible for the large instantaneous export fluxes. In contrast, the perturbation that maximizes integrated export (Φ_{INT}) is much less variable (Fig. 5). This result is contrary to the general expectation that systems with sporadic fluxes, such as coastal regions, have higher export (e.g., Harrison *et al.*, 1987).

For both non-optimal perturbations, $\Phi_{P_1 P_2}$ and Φ_{P_1}, the magnitude of the predator prey oscillations is larger than was the case for the optimal perturbations, and P_1 and D biomasses oscillate about steady state. The low P_2 biomass in these perturbations reduces grazing pressure of Z_2 on Z_1, allowing the microzooplankton to rapidly graze down the P_1 and terminate the bloom. The predator-prey cycles have a visible (but small) effect on N concentrations.

There are also similarities between the export responses to the optimal perturbations: all result in integrated export significantly above steady state (Table 4) such that the flux to higher trophic levels is the greatest contributor and aggregation is insignificant. The majority of export components remain above steady state in response to all optimal perturbations: anomalies in both Z_2 grazing on P_2, and sinking D remain positive (Fig. 5), and these fluxes are large enough to offset the decrease in Z_2 grazing when when Z_1 biomass ventures below steady state. The additional integrated export in response to Φ_{FLUX} and Φ_{FLUX-P} is 20% less than Φ_{INT} (Table 4), suggesting that as long as the perturbation is largely an increase in P_2, the other components do not significantly decrease the achievable export flux.

For both non-optimal perturbations ($\Phi_{P_1 P_2}$, Φ_{P_1}), sinking D and predation by Z_2 on Z_1 oscillate about steady state. Although increases in primarily P_1 result in export events with high instantaneous flux, the flux of P_2 to higher trophic levels is insufficient to offset these minima and keep net export above steady state.

The persistence of large phytoplankton has been found to be an important contributor to integrated export, both directly through sinking and grazing fluxes to Z_2, and indirectly through suppressing Z_1 biomass (through an increase in Z_2 specific grazing rate) allowing greater primary productivity by P_1. In nature, the P_2 decay time scales are likely to be much shorter due to dilution from advection and mixing. We note that our model setup is similar to that of GCMs, in that the horizontal resolution of these models is coarse relative to the physical exchanges being modeled. A consequence of the coarse resolution is that the importance of P_2 to export flux may be increased in the model relative to its importance in the natural system. Furthermore, the iron limitation parameter is held constant in this study, further increasing the persistence of P_2 blooms relative to those observed in nature (where iron limitation is not static). When iron limitation is considered in contemporary global biogeochemical models, iron limitation parameters vary spatially but not temporally

(e.g., Zahariev *et al.*, 2008), and it is possible that these models also overestimate primary production at some locations, and thus export.

It is generally believed that large phytoplankton are the primary contributor to export via flux to higher trophic levels and sinking particles (e.g., Michaels and Silver, 1988), even in conditions where primary production is dominated by small phytoplankton, so the fact that Φ_{INT} is an increase in only large phytoplankton is not surprising. However, the reasons for the increased export flux in response to this perturbation are counter-intuitive. While increasing P_2 does directly increase export flux, the main direct contribution of P_2 to export is through transfer to higher trophic levels rather than sinking and aggregation (Fig. 5c). Furthermore, a substantial portion of the sinking detritus comes from P_1, not P_2; at steady state, the P_1 contribution to detritus is four times as much as the P_2 contribution. The increase in large phytoplankton increases the grazing rate of mesozooplankton, leading to a depression in Z_1 and a bloom in P_1; the decline of this P_1 bloom is responsible for the increase in sinking detritus. Similarly a portion of the flux to higher trophic levels comes through the Z_1 and the organic matter in this flux originated from P_1.

In this model, small phytoplankton do not directly contribute to export flux Eq. (11), but P_1 do contribute to all components of export flux indirectly. A portion of P_1 that is grazed by the microzooplankton is not assimilated and becomes D, which sinks, forms aggregates, and is grazed on by Z_1. Some of the P_1 and D biomass that is assimilated by Z_1 will be exported to higher trophic levels as Z_2 graze on Z_1. Our analysis is consistent with the findings of Richardson and Jackson (2007), who suggest that the relative contributions of all phytoplankton to export, directly and indirectly, are proportional to their net primary production, and the importance of small phytoplankton to export flux may be underestimated in current models.

Export flux due to aggregation of microphytoplankton and detritus was found to make a negligible contribution to export flux in this study. Of course, this conclusion depends on the fidelity with which the process of aggregation is modeled. Full complexity dynamic coagulation models, that distinguish size classes of particles, have been embedded in a similar ecosystem model (the popular Fasham model; Fasham *et al.*, 1990). Results show that simple parameterizations of aggregation like ours are not capable of reproducing the results of the complex models and they suggest that aggregation is the most important contributor to particle export (Jackson, 2001). Ecosystem models, particularly those used in larger models, rarely include particle dynamics or even a simple form of aggregation. If the complex models are more capable of reproducing the natural system, it is possible that aggregation in models like the one used here is too simplistic. The results of Jackson (2001) bear directly on the partitioning of particle flux between sinking detritus and aggregation, but not on the partitioning of export between sinking particles and grazing by higher trophic levels. As a sensitivity test, we enhanced the impact of our simple parameterization, by increasing the aggregation coefficient, w_A, five fold to $0.1 \, \text{mmol} \, \text{N}^{-1} \, \text{m}^3 \, \text{d}^{-1}$ (Ruiz *et al.*, 2002) and found that it had a negligible effect on the ecosystem dynamics and optimal perturbations. In fact aggregation still remained the smallest contributor to export flux (not

shown). We also tried including the small phytoplankton in the aggregation term. Small particles would be expected to be caught by aggregates and the dynamic models suggest that small cells are an important contributor to aggregation in low particle density environments (e.g., Jackson, 2001; Jackson *et al.*, 2005). Again, although aggregation increased, it was still the least significant contributor to export for all experiments (on average about 15% of the total).

Clearly, the choice of zooplankton grazing function results in unexpected relationships between state variables, and the mathematical formulation of these functions is not well constrained by observations (Gentleman *et al.*, 2003). In the present model Z_1 are not allowed to graze on P_2; Denman *et al.* (2006) allow for this grazing pathway at a low preference. If this pathway were included in our model the relationships between the phytoplankton state variables could change. We use a simple and common formulation of the specific grazing rate (Holling type III). An alternate formulation could possibly eliminate some of the indirect relationships between planktonic classes not directly linked by a predator/prey relationship. This formulation also provides closure (through Z_2 grazing on Z_1) to our model (along with the linear Z_1 mortality term). The choice of closure term(s) has also been found to influence model dynamics, causing complex behaviour in some parameter space (Edwards and Yool, 2000).

In the analysis considered in this study, both the perturbation dynamics and perturbation export fluxes have been linearized. We tested the reasonableness of the assumption of locally linear dynamics by investigating the differences between the linear and nonlinear dynamics for perturbations of norm $0.5 \, \text{mmol N m}^{-3}$ (Healey, 2008). On the whole, the linearizations were qualitatively accurate approximations to the fully nonlinear dynamics, especially the linearization of export flux. Although there exists literature on nonlinear optimal perturbations (e.g., Mu *et al.*, 2003), the analysis of linear responses to perturbations ensures that results are independent of perturbation magnitude.

Although the perturbation Φ_{INT} is a large increase in P_2 biomass, $0.5 \, \text{mmol N m}^{-2}$ to 450% above steady state, diatom blooms of this magnitude have been observed at Station P. During the iron fertilisation experiment SERIES, microphytoplankton biomass increased from below $0.5 \, \text{mg Chl}a \, \text{m}^{-3}$ to over $3 \, \text{mg Chl}a \, \text{m}^{-3}$ (Marchetti *et al.*, 2006). Natural blooms with increases of this magnitude have also been observed at Station P (chl only; Harrison *et al.*, 1999) and in the HNLC equatorial Pacific (specifically diatoms; Friedrich and Hofmann, 2001).

According to this model, an event that increases P_2 by $0.5 \, \text{mmol N m}^{-2}$ could enhance integrated export (via the biological pump) by 30% ($7.4 \, \text{g C m}^{-2}$) above steady state over the summer season (two-three months). In part this increase is due to the persistence of P_2 that is characteristic to the model, and would be expected to be similar were this model embedded in a GCM although it may not be realistic (discussed above). Extending this result to the entire HNLC region of the world ocean, this perturbation would increase carbon export by $0.5 \, \text{Pg C}$. It is estimated that $8.5 \, \text{Pg C}$ was exported in 2007. Thus, this model predicts that diatom blooms in HNLC regions could be a significant contributor to global carbon export,

depending on how readily environmental fluctuations generate perturbations close to those which optimize export.

5. Conclusions

This study has considered the response of an idealized, common planktonic ecosystem model to perturbations in the initial conditions. In particular, an analysis of the linearized dynamics around a stable steady state of the system, that is similar to observations of the natural system, allowed the diagnosis of those initial perturbations which resulted in maximum amplification of instantaneous export flux and those which resulted in maximum net export over the duration of the perturbation. The following primary results were obtained:

- Perturbations to planktonic ecosystems may display dramatic transient growth, as measured by export flux, and a consideration of dynamics linearized locally around a steady stable state allows the computation of those perturbations which lead to the largest export response.
- There is no simple relationship between amplification, maximum instantaneous export flux, and integrated export flux. Some perturbations resulted in a high initial increase in export but did not have significant net export flux, others had large net flux but not strong amplification. Thus, this model does not support the generalization that systems with strong sporadic blooms lead to the highest export production.
- This study reinforces the notion that the complexity of interactions between components even in a linearized model cannot be ignored; important aspects of the ecosystem responses such as export flux were sensitive to the structure of the perturbations.
- Small zooplankton played a critical role in modeled fluxes due to its direct and indirect role in trophic transfers (by modulating the grazing of P_2 by Z_2, see Results). In general, microzooplankton are poorly sampled and their role in observed ocean ecosystem is not well understood (relative to those of other components of the ecosystem). The results of this study provide further support for more detailed observation of this component of the ecosystem.
- The flux to higher trophic levels is not well understood and so model representations are often arbitrary. However this research showed that the flux to higher trophic levels was the dominant contributor to export flux rather than sinking particles. Furthermore, aggregation played an insignificant role. This result could in part be an artifact of the ecosystem model, however it was robust for all experiments even when the aggregation term was enhanced or P_1 was allowed to aggregate.
- The small phytoplankton were shown to play a significant role in exported carbon, consistent with new observational studies (Richardson and Jackson, 2007). The indirect contribution of small phytoplankton to export flux was comparable to the contribution of the large phytoplankton.

This analysis yields relationships between state variables that are not obvious. It would be useful to investigate how export dynamics would change were a different ecosystem

model used, particularly a model with different grazing formulations and trophic interactions. Results could elucidate key differences between models and give an indication of the generality of the conclusions obtained with the present model. Another natural extension of this study would be to perform a similar analysis on an ecosystem model that includes different carbon compounds, and a functional group of calcifying phytoplankton, whose importance is becoming increasingly recognized as a consequence of ocean acidification. Furthermore, this model is set in the open ocean, and the parameters are tuned for a HNLC area where the effects of nutrient limitation are assumed constant. Because the ecosystem was not N limited in steady state, the response of N to perturbations did not affect the dynamics of other state variables. This type of analysis could be used to study the transient dynamics of other open ocean regions or coastal ecosystem models, which may be limited by N, and possibly other nutrients, and are subject to different sources of perturbations.

This study has assumed that both the physical environment and the biomass of the uppermost trophic level (Z_2) remain constant in time, when in reality both can display diurnal and seasonal cycles as well as irregular, unpredictable variability in response to external "weather" (e.g., Monahan and Denman, 2004). Accounting for seasonal variability in the physical environment (e.g., mixed layer depth and surface solar flux) and the Z_2 biomass would influence the long-time evolution of the perturbation (i.e., on timescales greater than 60 days), but are less relevant for the shorter timescale behaviour. The perturbation dynamics on timescales of greater than two or three months are not realistic; however, the dominant perturbation responses of all state variables except N are contained within this time period. External "weather" variability plays an important role in driving the planktonic system away from equilibrium, generating the initial perturbations the response to which is the focus of this study. This analysis can be extended to account for both smooth (e.g., diurnal, seasonal) and irregular external forcing (e.g., Farrell and Ioannou, 1996a,b); such an extension would be an interesting direction for future research.

Of the various perturbations considered, that most relevant to the biological pump is the perturbation that maximizes total export. For the present model, this optimal perturbation is confined almost entirely to the large phytoplankton; this result could have been obtained in a more straightforward (and more computationally intensive) manner by integrating the dynamics for an appropriate range of initial conditions. The primary drawback with this simpler approach is that the neighbourhood of the truly optimal perturbation may not be adequately sampled. With sufficient computational power, the space of initial conditions can be reasonably well sampled for models with a small number of state variables such as the one under consideration. However, the density of coverage drops exponentially as the number of variables increases; even a small increase in the complexity of the model can dramatically reduce the representativeness of the set of initial conditions. The optimal perturbation approach considered in this study is completely general and allows direct computation of those perturbations that excite maximal responses in systems ranging from the very simple to the very complex.

The response of this ecosystem model to perturbations provides insight into how planktonic ecosystems may respond to natural variability, and how ecosystem models may respond to a changing environment when coupled with GCMs. Because these models are being used to predict future climate scenarios, it is important to study their internal dynamics and the effects of these dynamics on carbon fluxes in ocean models.

APPENDIX A

Model description

The planktonic ecosystem model considers two functional groups of phytoplankton: nanophytoplankton (flagellates, P_1) and microphytoplankton (diatoms, P_2), two functional types of zooplankton; microzooplankton (Z_1) and mesozooplankton (Z_2, which is specified), and detritus (D). The single prognostic nutrient is nitrogen (N), which is also the model currency. The evolution of these five state variables is given by the following set of differential equations:

$$\frac{dP_1}{dt} = \underbrace{vP_1}_{growth} - \underbrace{\gamma_1 \frac{P_1}{P_1 + p_D D} Z_1}_{Z_1\ grazing\ on\ P_1} \tag{3}$$

$$\frac{dP_2}{dt} = \underbrace{vP_2}_{growth} - \underbrace{\gamma_2 Z_2 \frac{P_2}{P_2 + Z_1}}_{Z_2\ grazing\ on\ P_2} - \underbrace{m_{pd} P_2}_{mortality} - \underbrace{w_A(P_2^2 + \frac{2P_2}{P_2 + D} P_2 D)}_{aggregation} \tag{4}$$

$$\frac{dZ_1}{dt} = \underbrace{g_a \gamma_1 Z_1}_{growth} - \underbrace{\gamma_2 Z_2 \frac{Z_1}{P_2 + Z_1}}_{Z_2\ grazing\ on\ Z_1} - \underbrace{m_{za} Z_1}_{mortality} \tag{5}$$

$$\frac{dD}{dt} = \underbrace{m_{pd} P_2}_{P_2\ mortality} + \underbrace{(1 - g_a)\gamma_1 Z_1}_{Z_1\ ``sloppy\ feeding"} - \underbrace{\gamma_1 \frac{p_D D}{P_1 + p_D D} Z_1}_{Z_1\ grazing\ on\ D}$$

$$- \underbrace{r_e D}_{remineralization} - \underbrace{w_D D}_{sinking} - \underbrace{w_A(D^2 + \frac{2D}{P_2 + D} P_2 D)}_{aggregation} \tag{6}$$

$$\frac{dN}{dt} = \underbrace{-v(P_1 + P_2)}_{P\ growth} + \underbrace{r_e D}_{remineralization} + \underbrace{m_{za} Z_1}_{Z_1\ mortality} + \underbrace{m_{ca} \gamma_2 Z_2}_{Z_2\ excretion} + \underbrace{\frac{v_{UW}}{d_{ML}}(N_0 - N)}_{upwelling} \tag{7}$$

Table 5. Model parameter values. Many ecosystem parameters have been tuned to agree with observations and are not well constrained. MD04=Monahan and Denman (2004), DP02=Denman and Pena (2002), W99=Whitney and Freeland (1999), A93= Archer *et al.* (1993), CV=C. Voelker, pers. com., P-Hist=Station P historical data, Institute of Ocean Sciences Archive.

		Value	Unit	Source
v_{max}	maximum phyto. growth rate	1.5	d^{-1}	DP02
p_d	grazing preference of Z_1 on D	0.5	-	DP02
Z_2	Z_2 biomass	0.2	mmol N m^{-3}	DP02
m_{pd}	P_2 to D mortality	0.1	d^{-1}	MD04
m_{za}	Z_1 to N	0.1	d^{-1}	MD04
r_e	D remineralization rate	0.1	d^{-1}	DP02
m_{ca}	Z_2 grazing to N	0.3	-	DP02
r_m	maximum Z_1 grazing rate	1.0	d^{-1}	DP02
k_p	Z_1 grazing half-saturation const.	0.75	mmol N m^{-3}	DP02
r_c	maximum Z_2 grazing rate	6.5	d^{-1}	MD04
k_z	Z_2 grazing half-saturation const.	2	mmol N m^{-3}	MD04
N_0	average N below mixed layer	26.8	mmol N m^{-3}	P-Hist
k_n	P growth half-saturation const.	0.1	mmol N m^{-3}	DP02
L_{fe}	iron limitation coefficient	0.05	-	tuned
d_{ML}	mixed layer depth	20	m	W99
v_{uw}	upwelling velocity	.1	m d^{-1}	A93
w_D	D turnover rate due to sinking	0.3750	d^{-1}	MD04
g_a	Z_1 assimilation efficiency	0.7	-	DP02
w_A	aggregation coefficient	0.02	mmol N^{-1} m^3 d^{-1}	CV

The parameter values used in this study are given in Table 5. The phytoplankton specific growth rate, v, is given by Liebig's law of the minimum:

$$v = v_{max} min\left(\frac{N}{k_n + N}, L_{fe}\right) \tag{8}$$

where v_{max} is the maximum growth rate in the absence of nutrient limitation and k_N is a nitrogen half-saturation constant. When growth is not limited by N, the parameter L_{fe} sets an upper limit on phytoplankton growth that represents limitation of a micronutrient such as iron. Because the model is set in summer conditions, it is assumed that light is not limiting at any time.

The microzooplankton, Z_1, graze on both P_1 and D with grazing rate

$$\gamma_1 = r_m \frac{(P_1 + p_D D)^2}{k_p^2 + (P_1 + p_D D)^2} \tag{9}$$

where p_D is the relative grazing preference of Z_1 on D over P_1 and k_p is the "half-saturation constant".

Mesozooplankton biomass is held fixed because Z_2 have relatively long life spans (order months to years) compared to Z_1, and biomass is unlikely to change in response to ecosystem changes on the time scales considered. However, the Z_2 grazing rate responds to changes in availability of P_2 and Z_1:

$$\gamma_2 = r_c \frac{(P_2 + Z_1)^2}{k_z^2 + (P_2 + Z_1)^2} \tag{10}$$

The mortality rate of P_2 to D, m_{pd}, is linear. Aggregation, i.e., the formation of marine snow (Alldredge and Silver, 1988), is represented by a quadratic term in both P_2 and D. The assimilation efficiency of Z_1, i.e., the portion of grazed P that is converted to Z biomass, is denoted g_a; unassimilated matter, e.g., biomass lost to sloppy feeding, becomes D. Microzooplankton excrete N with specific rate m_{za}. The particulate nitrogen contained in detritus is converted to dissolved nitrogen at the specific remineralization rate r_e, and D sinks at rate w_D (7.5 m d^{-1}). A portion of the biomass grazed by Z_2 is immediately excreted to N at a rate of m_{ca}.

Station P is located in the Alaskan Gyre, a region of weak upwelling (Pond and Pickard, 1983). Nitrogen is injected via upwelling and exchanged by mixing with water from below the mixed layer that has average nitrogen concentration N_0 at rate v_{UW}. Any dilution of other state variables by physical exchange is included in the linear growth and mortality rates. The physical parameters for the model are set to be broadly consistent with observations made at Station P in the summer, for those parameters for which these observations exist (Table 5).

APPENDIX B

Export

In this study, we determine perturbations that maximize export from the ecosystem described in Eqs. 3-7. This export is given by the equation

$$Export = w_D D + (1 - m_{ca})\gamma_2 Z_2 + w_A (P_2 + D)^2$$

The sinking D export flux depends linearly on D, however the flux to higher trophic levels and aggregation terms are nonlinear and so must be linearized about the steady state in order to perform the optimizations described in Appendix C. The export function for the ecosystem state is approximated using a Taylor series expansion:

$$Export(\mathbf{x}_0 + \Delta\mathbf{x}) \approx Export(\mathbf{x}_0) + \nabla Export(\mathbf{x}_0)^T \cdot \Delta\mathbf{x} \tag{11}$$

where $\mathbf{x}_0$ is the ecosystem steady state, $\Delta\mathbf{x}$ the perturbation to this state, and ∇ the gradient operator relative to the state variables. The linearized export is thus given by the equation

$$Export = Export(\mathbf{x}_0) + 0.22\Delta P_2 + 0.21\Delta Z_1 + 0.38\Delta D$$

where ΔP_2, ΔZ_1, and ΔD are the perturbations in large phytoplankton, small zooplankton, and detritus, respectively. The export rates are computed in units of $\mathrm{mmol\,N\,m^{-3}d^{-1}}$ and a constant C:N ratio is assumed for P_2, Z_1, and D, so comparing nitrogen export rates is equivalent to comparing the carbon export rate. The Redfield C:N ratio for phytoplankton of 106:16 is used (Redfield *et al.*, 1963). Note that C:N may vary in time and for different forms of organic matter in the ocean, but on average it is well approximated by the Redfield ratio. Variations in the ratio are not modeled because the added complexity is not warranted or well-constrained (Sterner and Elser, 2002).

APPENDIX C

Optimal perturbations

Because this study focuses on the linearized dynamics of the nonlinear planktonic ecosystem model described in Eqs. (3)-(7), we include a brief background on the linearization of these differential equations. More details can be found in standard undergraduate textbooks on systems of differential equations (e.g., Perko, 2001).

The system of Eqs. (3)-(7) can be expressed as the autonomous system of first order ordinary differential equations

$$\frac{d\mathbf{x}}{dt} = \mathbf{f}(\mathbf{x}) \tag{12}$$

where $\mathbf{x} = (P_1, P_2, Z_1, D, N)$ is the state vector. The dynamics of a small perturbation around a fixed point $\mathbf{x}_0$, $\Delta\mathbf{x} = \mathbf{x} - \mathbf{x}_0$, can be described by the linearized dynamics

$$\frac{d}{dt}\Delta\mathbf{x} = \mathbf{A}\Delta\mathbf{x}, \tag{13}$$

where $\mathbf{A}$ is the Jacobian of $\mathbf{f}(\mathbf{x})$ evaluated at $\mathbf{x}_0$, that is

$$A_{i,j} = \frac{\partial f_i(\mathbf{x})}{\partial x_j}\Big|_{\mathbf{x}=\mathbf{x}_0}. \tag{14}$$

If $\mathbf{A}$ is diagonalizable, the solution of Eq. (13) is

$$\Delta\mathbf{x}(t) = e^{At}\Delta\mathbf{x}_0. \tag{15}$$

Provided that $\mathbf{x}$ remains sufficiently close to $\mathbf{x}_0$, the linearized dynamics will be a good approximation to the evolution of the full nonlinear system.

a. Optimizing rates

If the equilibrium $\mathbf{x}_0$ is stable, then the real parts of the eigenvalues of $\mathbf{A}$ will all be negative and small perturbations to a stable steady state will eventually converge back to equilibrium. However, these perturbations may display transient growth over finite times if these eigenvalues are complex.

The solution to Eq. 13 is a superposition of the eigenmodes of $\mathbf{A}$. The eigenmodes of a normal matrix (i.e., $\mathbf{A}\mathbf{A}^T = \mathbf{A}^T\mathbf{A}$, where $\mathbf{A}^T$ is the transpose of $\mathbf{A}$ (Farrell and Ioannou, 1996a)) $\mathbf{A}$ are orthogonal, and if all eigenvalues of $\mathbf{A}$ are negative, any perturbation $\Delta\mathbf{x}_0$ from stable steady state will decay monotonically. However, if $\mathbf{A}$ is non-normal, constructive interference between non-orthogonal eigenmodes can allow for transient growth over finite times (although the ecosystem returns asymptotically to the stable steady state). Non-normality of the linearized model is expected to be the norm for ecosystem models. For example, in the present model, interactions between P_1 and Z_1 are not symmetric as not all grazed phytoplankton biomass is assimilated as zooplankton biomass. This ecological asymmetry results in an asymmetric (and non-normal) linearized dynamical operator.

It is possible to solve for the perturbation of a given norm (under some metric) that maximizes some measure of the size of the perturbation at a fixed time τ at time $t = 0$ (Tziperman and Ioannou, 2002). Under linear dynamics, the magnitude of the response is proportional to that of the initial perturbation. The goal of the present analysis is to determine, among all perturbations of the same initial magnitude (as measured by the norm S), those perturbations which result in a maximum response (as measured by the norm R, which will in general differ from S) at some later time. Mathematically, this is expressed as a constrained optimization problem.

Let $\mathbf{R}$ be a matrix defining the perturbation norm to be maximized, so that the magnitude of the perturbation at time τ is given by

$$J(t) = \Delta\mathbf{x}_0^T (e^{A\tau})^T \mathbf{R} e^{A\tau} \Delta\mathbf{x}_0. \tag{16}$$

The optimal perturbation at time τ is defined as the initial perturbation $\Delta\mathbf{x}_0$ that maximizes $J(\tau)$ under the norm $\mathbf{R}$, subject to the constraint that the norm of this perturbation is constant under some nonsingular norm $\mathbf{S}$. In this study, we solve for perturbations of unit norm:

$$\Delta\mathbf{x}_0^T \mathbf{S} \Delta\mathbf{x}_0 = 1. \tag{17}$$

It follows from this constrained optimization problem that the optimal perturbations satisfy the generalized eigenvalue problem

$$(e^{A\tau})^T \mathbf{R} e^{A\tau} \Delta\mathbf{x}_0 = \lambda \mathbf{S} \Delta\mathbf{x}_0 \tag{18}$$

where λ, the Lagrange multiplier introduced by the unit-norm constraint (Eq. (17)), takes on the values of the eigenvalues of matrix

$$\mathbf{S}^{-1}(e^{A\tau})^T \mathbf{R} e^{A\tau} \tag{19}$$

and the eigenvector corresponding to the eigenvalue λ with greatest real part is the optimal perturbation at time τ under the norm $\mathbf{R}$. As the perturbation evolves, the amplification of

the perturbation under $\mathbf{R}$ is defined as the magnitude of the state vector under $\mathbf{R}$ relative to the initial magnitude of the state vector under $\mathbf{R}$:

$$Amp^2(t) = \frac{\Delta\mathbf{x}(t)^T \mathbf{R}\Delta\mathbf{x}(t)}{\Delta\mathbf{x}_0^T \mathbf{R}\Delta\mathbf{x}_0}. \tag{20}$$

Because the export has been linearized, the square of the export is

$$Export^2(\mathbf{x}) = (0.22\Delta P_2 + 0.21\Delta Z_1 + 0.38\Delta D)^2 = (a_1 x_1 + a_2 x_2 + .. + a_5 x_5)^2 = \mathbf{x}^T \mathbf{R}\mathbf{x} \tag{21}$$

so $R_{i,j} = a_i a_j$. We have chosen to look for those perturbations which maximize export among all perturbations of "unit norm" in biomass, so the constraint on the initial condition takes the form of Eq. (17).

The instantaneous export flux is maximized subject to the constraint that the initial biomass of the perturbation is unity. For the perturbation in all state variables, Φ_{FLUX}, $\mathbf{S}$ is the identity matrix, and all state variables are weighted equally in the perturbation constraint. For Φ_{FLUX-P}, entries in $\mathbf{S}$ involving state variables other than P_1 and P_2 are large to suppress contributions of the other state variables.

b. Optimizing integrated quantities

The above theory is used to maximize the magnitude of the instantaneous state of a system of equations under some measure. Because of the potential of planktonic ecosystems as carbon sinks, it is of interest to determine the perturbation that results in the maximum carbon export over some period of time, that is, the integrated export. Maximizing the instantaneous export flux is equivalent to maximizing its square (Eq. (16)). However, the perturbation that maximizes the integral of the squared export flux does not necessarily result in the highest integrated export (which might involve some cancellation between positive and negative anomalies in export flux), so a different approach is required. The previous optimization problem involves a bilinear operator in the state vector, whereas this problem maximizes a dot product, and is linear in the state vector. An analogous optimization problem was considered by DelSole (2001); the following analysis is based on the results of this earlier study.

It is possible to determine the unit perturbation $\Delta\mathbf{x}_0$ that maximizes the integral of the projection of the model state on some vector $\mathbf{y} = (y_1, y_2, \ldots, y_n)$, where n is the dimension of the model. The quantity to be maximized (in the present case, the export flux) is

$$\int_0^\infty \mathbf{y} \cdot e^{At}\Delta\mathbf{x}_0 dt \approx \Delta t \sum_{\tau=0}^\infty \mathbf{y} \cdot e^{A\tau\Delta t}\Delta\mathbf{x}_0 \tag{22}$$

where Δt is the timestep. Including the intitial condition constraint, we maximize

$$I = \Delta t \sum_{\tau=0}^{\infty} \mathbf{y} \cdot e^{A\tau\Delta t} \Delta \mathbf{x}_0 + \lambda (\Delta \mathbf{x}_0^T \mathbf{S} \Delta \mathbf{x}_0 - 1) \tag{23}$$

where λ is a Lagrange multiplier, and $\mathbf{S}$ is the identity matrix, as in Appendix C. Let $M(\tau) = e^{A\tau\Delta t}$. Expanding Eq. (23)

$$I = \Delta t \sum_{\tau=0}^{\infty} \mathbf{y} \cdot \begin{bmatrix} M_{11}\Delta x_{0_1} + \cdots + M_{n1}\Delta x_{0_n} \\ \cdot \\ \cdot \\ M_{n1}\Delta x_{0_1} + \cdots + M_{nn}\Delta x_{0_n} \end{bmatrix} + \lambda (\Delta \mathbf{x}_0^T \mathbf{S} \Delta \mathbf{x}_0 - 1) \tag{24}$$

and setting the gradient with respect to $\Delta \mathbf{x}_0$ to $\mathbf{0}$

$$\begin{bmatrix} \Delta t \sum_{\tau=0}^{\infty} (y_1 M_{11} + \cdots + y_n M_{n1}) \\ \cdot \\ \cdot \\ \Delta t \sum_{\tau=0}^{\infty} (y_1 M_{1n} + \cdots + y_n M_{nn}) \end{bmatrix} + 2\lambda \begin{bmatrix} \Delta x_{0_1} \\ \cdot \\ \cdot \\ \Delta x_{0_n} \end{bmatrix} = \begin{bmatrix} 0 \\ \cdot \\ \cdot \\ 0 \end{bmatrix} \tag{25}$$

yields

$$\Delta x_{0j} = \frac{\Delta t}{2\lambda} \sum_{\tau=1}^{\infty} \sum_{i=1}^{n} y_i M_{i,j}(\tau) \tag{26}$$

The Lagrange multiplier λ is determined through the requirement that $\Delta \mathbf{x}_0$ be of unit norm.

Note that optimizing the integrated export over the interval $[\tau - \Delta, \tau + \Delta]$ is equivalent to optimizing the instantaneous export flux at time τ as $\Delta \to 0$.

REFERENCES

Alldredge, A. and M. Silver. 1988. Characteristics, dynamics and significance of marine snow. Prog. Oceanogr., *20*, 41–82.

Archer, D., S. Emerson, T. Powell, and C. Wong. 1993. Numerical hindcasting of sea surface pCO$_2$ at weathership Station Papa. Prog. Oceanogr., *32*, 319–351.

Boyd, P. and P. Harrison. 1999. Phytoplankton dynamics in the NE subarctic Pacific. Deep-Sea Res. II, *46*, 2405–2432.

Boyd, P. W., C. S. Law, C. S. Wong, Y. Nojiri, A. Tsuda, M. Levasseur, S. Takeda, R. Rivkin, P. J. Harrison, R. Strzepek, J. Gower, R. M. McKay, E. Abraham, M. Arychuk, J. Barwell-Clarke, W. Crawford, D. Crawford, M. Hale, K. Harada, K. Johnson, H. Kiyosawa, I. Kudo, A. Marchetti, W. Miller, J. Needoba, J. Nishioka, H. Ogawa, J. Page, M. Robert, H. Saito, A. Sastri, N. Sherry, T. Soutar, N. Sutherland, Y. Taira, F. Whitney, S. K. E. Wong, and T. Yoshimura. 2004. The decline and fate of an iron-induced subarctic phytoplankton bloom. Nature, *428*, 549–553.

de Baar, H., P. Boyd, K. Coale, M. Landry, A. Tsuda, P. Assmy, D. Bakker, Y. Bozec, R. Barber, M. Brzezinski, K. Buesseler, M. Boye, P. Croot, F. Gervais, M. Gorbunov, P. Harrison, W. Hiscock,

P. Laan, C. Lancelot, C. Law, M. Levasseur, A. Marchetti, F. Millero, J. Nishioka, Y. Nojiri, T. van Oijen, U. Riebesell, M. Rijkenberg, H. Saito, S. Takeda, K. Timmermans, M. Veldhuis, A. Waite, and C.-S. Wong. 2005. Synthesis of iron fertilization experiments: From the iron age in the age of enlightenment. J. Geophys. Res., *110*, 1–24.

DelSole, T. 2001. Optimally persistent patterns in time-varying fields. J. Atmos. Sci., 58, 1341–1356.

Denman, K. and M. Pena. 2002. The response of two coupled one-dimensional mixed layer/planktonic ecosystem models to climate change in the NE subarctic Pacific Ocean. Deep-Sea Res. II, *49*, 5739–5757.

Denman, K. L., C. Voelker, M. A. Pena, and R. B. Rivkin. 2006. Modelling the ecosystem response to iron fertilization in the subarctic NE Pacific: The influence of grazing, and Si and N cycling on CO_2 drawdown. Deep-Sea Res. II, *53*, 2327–2352.

Edwards, A. M. and J. Brindley. 1999. Zooplankton mortality and the dynamical behaviour of plankton population models. Bull. Math. Biol., *61*, 303–339.

Edwards, A. M. and A. Yool. 2000. The role of higher predation in plankton population models. J. Plankton Res., *22*, 1085–1112.

Farrell, B. and P. Ioannou. 1996a. Generalized stability theory. Part 1: Autonomous operators. J. Atmos. Sci., *53*, 2025–2040.

———. 1996b. Generalized stability theory. Part 2: Nonautonomous operators. J. Atmos. Sci., *53*, 2041–2053.

Fasham, M. J. R. 1993. Modelling the marine biota, in The Global Carbon Cycle, M. Heimann, ed., Springer-Verlag, 457–504.

Fasham, M. J. R., H. W. Ducklow, and S. M. McKelvie. 1990. A nitrogen-based model of plankton dynamics in the oceanic mixed layer. J. Mar. Res., *48*, 591–639.

Friedrich, M. A. M. and E. E. Hofmann. 2001. Physical control of biological processes in the central equatorial Pacific Ocean. Deep Sea Res. I, *48*, 1023–1069.

Gentleman, W., A. Leising, B. Frost, S. Strom, and J. Murray. 2003. Functional responses for zoo-plankton feeding on multiple resources: a review of assumptions and biological dynamics. Deep-Sea Res. II, *50*, 2847–2875.

Goldblatt, R. H., D. L. Mackas, and A. G. Lewis. 1999. Mesozooplankton community characteristics in the NE subarctic Pacific. Deep-Sea Res. II, *46*, 2619–2644.

Harrison, P. J., P. W. Boyd, D. E. Varela, S. Takeda, S. A., and T. Odated. 1999. Comparison of factors controlling plankton productivity in the NE and subarctic Pacific gyres. Prog. Oceanog., *43*, 205–234.

Harrison, W. G., T. Platt, and M. R. Lewis. 1987. f-ratio and its relationship to ambient nitrate concentration in coastal waters. J. Plankton Res., *9*, 235–248.

Healey, K. 2008. Perturbation Dynamics of a Planktonic Ecosystem, Master's thesis, University of Victoria.

Jackson, G. A. 2001. Effect of coagulation on a model planktonic food web. Deep-Sea Res. I, *48*, 95–123.

Jackson, G. A., A. M. Waite, and P. W. Boyd. 2005. Role of algal aggregation in vertical carbon export during SOIREE and in other low biomass environments. Geophys. Res. Lett., *32*, L13607, doi:10.1029/2005GL023180.

Jo, C. O., J. Y. Lee, K. A. Park, Y. H. Kim, and K. R. Kim. 2007. Asian dust initiated early spring bloom in the northern East/Japan Sea. Geophys. Res. Lett., *34*.

Leising, A. W., W. C. Gentleman, and B. W. Frost. 2003. The threshold feeding response of microzoo-plankton within Pacific high-nitrate low-chlorophyll ecosystem models under steady and variable iron input. Deep-Sea Res. II, *50*, 2877–2894.

Marchetti, A., N. D. Sherry, P. Juneau, R. F. Strzepek, and P. J. Harrison. 2006. Phytoplankton processes during a mesoscale iron enrichment in the NE subarctic Pacific: Part III Primary productivity. Deep-Sea Res. II, *53*, 2131–2151.

Martin, J., R. Gordon, and S. Fitzwater. 1991. The case for iron. Limnol. Oceanogr., *36*, 1793–1802.

Martin, J., R. Gordon, S. Fitzwater, and W. Broenkow. 1989. VERTEX: Phytoplankton/iron studies in the Gulf of Alaska. Deep-Sea Res., *36*, 649–680.

McGillicuddy, D. J., A. R. Robinson, and J. J. McCarthy. 1995. Coupled physical and biological modelling of the spring bloom in the North Alantic (II): three dimensional bloom and post-bloom processes. Deep-Sea Res. I, *42*, 1359–1398.

Michaels, A. F. and M. W. Silver. 1988. Primary production, sinking fluxes and the microbial food web. Deep-Sea Res., *35*, 473–490.

Monahan, A. and K. Denman. 2004. Impacts of atmospheric variability on a coupled upper-ocean/ecosystem model of the subarctic Northeast Pacific. Global Biogeochem. Cycles, *18*, GB2010, doi:10.1029/2003GB002100.

Moore, J. K., S. C. Doney, and K. Lindsay. 2004. Upper ocean ecosystem dynamics and iron cycling in a global three-dimensional model. Global Biogeochem. Cycles, *18*, 1–21.

Mu, M., W. S. Duan, and B. Wang. 2003. Conditional nonlinear optimal perturbation and its applications. Nonlinear Proc. Geophys., *10*, 493–501.

Perko, L. 2001. Differential Equations and Dynamical Systems, Springer-Verlag, 538 pp.

Pitchford, J. W. and J. Brindley. 1999. Iron limitation, grazing pressure and oceanic high nutrient-low chlorophyll (HNLC) regions. J. Plankton Res., *21*, 525–547.

Pond, S. and G. L. Pickard. 1983. Introductory Dynamical Oceanography, Butterworth-Heinemann, 349 pp.

Redfield, A. C., B. H. Ketchum, and F. A. Richards. 1963. The influence of organisms on the composition of sea-water, in The Sea: Ideas and Observations on Progress in the Study of the Seas, M. Hill, ed., John Wiley and Sons, NY, 26–77.

Richardson, T. L. and G. A. Jackson. 2007. Small phytoplankton and carbon export from the surface ocean. Science, *315*, 838–840.

Ruiz, J., L. Prieto, and F. Ortegon. 2002. Diatom aggregate formation and fluxes: a modeling analysis under different size-resolution schemes and with empirically determined aggregation kernels. Deep-Sea Res. I, *49*, 495–515.

Saito, H., A. Tsuda, Y. Nojiri, J. Nishioka, S. Takeda, H. Kiyosawa, I. Kudo, Y. Noiri, T. Ono, Y. Taira, K. Suzuki, T. Yoshimura, and P. W. Boyd. 2006. Nutrient and phytoplankton dynamics during the stationary and declining phases of a phytoplankton bloom induced by iron-enrichment in the eastern subarctic Pacific. Deep-Sea Res. II, *53*, 2168–2181.

Sarmiento, J. L. and N. Gruber. 2006. Ocean Biogeochemical Dynamics, Princeton University Press, 526 pp.

Schmittner, A., A. Oschlies, X. Giraud, M. Eby, and H. Simmons. 2005. A global model of the marine ecosystem for long-term simulations: Sensitivity to ocean mixing, buoyancy forcing, particle sinking, and dissolved organic matter cycling. Global Biogeochem. Cycles, *19*, 1–17.

Steele, J. 1974. The Structure of Marine Ecosystems, Harvard University Press, 128 pp.

Sterner, R. W. and J. J. Elser. 2002. Ecological Stoichiometry: The Biology of Elements from Molecules to the Biosphere, Princeton University Press, 584 pp.

Truscott, J. E. and J. Brindley. 1994. Ocean plankton populations as excitable media. Bull. Math. Biol., *56*, 981–998.

Tziperman, E. and P. J. Ioannou. 2002. Transient growth and optimal excitation of thermohaline variability. J. Phys. Oceanogr., *32*, 3427–3435.

Volk, T. and M. Hoffert. 1985. Ocean carbon pumps - Analysis of relative strengths and efficiencies in ocean-driven atmospheric CO_2 changes, in The Carbon Cycle and Atmospheric CO_2: Natural Variations Archean to Present, *Geophysical Monograph Series*, 32, E. Sundquist, and W. Broecker, eds., AGU, Washington, D.C., 99–110.

Volterra, V. 1928. Variations and fluctuations of the number of individuals in animal species living together. ICES J. Mar. Sci., *3*, 3–51.

Whitney, F. and H. Freeland. 1999. Variability in upper-ocean water properties in the NE Pacific Ocean. Deep-Sea Res. II, *46*, 2351–2370.

Whitney, F. A. and P. D. Tortell. 2006. Fifty years of ocean observations in the Pacific Northeast. EOS Trans., AGU, *87*, 551, doi:10.1029/2006EO490005.

Wong, C. S., D. A. Timothy, C. S. Law, Y. Nojiri, L. S. Xie, S. K. E. Wong, and J. S. Page. 2006. Carbon distribution and fluxes during the SERIES iron fertilization experiment with special reference to the fugacity of carbon dioxide (fCO_2). Deep-Sea Res. II, *53*, 2053–2074.

Wong, C. S., F. A. Whitney, D. W. Crawford, K. Iseki, R. J. Matear, W. K. Johnson, and J. S. Page. 1999. Seasonal and interannual variability in particle fluxes of carbon, nitrogen and silicon from time series of sediment traps at Ocean Station P, 1982-1993: relationship to changes in subarctic primary productivity. Deep-Sea Res. II, *46*, 2735–2760.

Zahariev, K., J. Christian, and K. Denman. 2008. A global ocean carbon model with novel parameterizations of iron limitation, calcification and N_2 fixation: preindustrial, historical, and fertilization simulations. Prog. Oceanogr., *77*, 56–82.